$^2A'$ and $^2A''$ Energy Surfaces for the Sc + CO_2 → ScO + CO Reaction

Imre Pápai* and Gábor Schubert

Institute of Chemistry, Theoretical Chemistry Department, Chemical Research Centre of HAS, Pusztaszeri út 59-67, H-1025 Budapest, Hungary

Yacine Hannachi* and Joëlle Mascetti

Laboratoire de Physico-Chimie Moléculaire (UMR 5803 CNRS), Université Bordeaux I, 351, cours de la Libération, 33405 Talence Cedex, France

Received: April 10, 2002; In Final Form: June 10, 2002

The mechanism of the title reaction has been investigated using density functional and coupled cluster calculations. The results indicate that the lowest energy path corresponds to the η^2_{CO} coordination of CO_2 followed by the insertion of Sc into a C−O bond. We show that two doublet state ($^2A'$ and $^2A''$) potential energy surfaces have to be considered to describe the reaction mechanism. On the $^2A'$ surface, the reaction gives a weakly bound OScCO species that can easily dissociate into ground state ScO($^2\Sigma^+$) + CO products, whereas the $^2A''$ state insertion complex is thermodynamically stable because it correlates to an excited state of ScO. The applicability of the B3LYP and CCSD(T) methods for the relative stability of intermediates is examined, and our results are related to available experimental findings.

I. Introduction

Because of their relevance to catalytic CO_2 activation,[1−4] reactions of transition metal atoms with carbon dioxide have been extensively studied both experimentally[5−22] and theoretically.[16−35] Matrix isolation experiments revealed a diverse behavior of the first row transition metal atoms in the reactions with CO_2.[14] It has been shown in these experiments that thermally evaporated metals from the left-hand side of the series insert spontaneously into CO_2 giving rise to metal−oxide−carbonyl (OMCO) complexes, whereas the late transition metals form only relatively weak M(CO_2) addition complexes. The OMCO type insertion complexes have been later produced for the entire Sc−Ni series,[15−19] as well as for a few 4d and 5d metals,[20−22] by reacting laser-ablated metals with carbon dioxide. The gas phase kinetics of the full oxygen abstraction reaction (M + CO_2 → MO + CO) have also been studied experimentally using a laser photolysis/laser-induced fluorescence technique, and the bimolecular reaction rate constants along with the reaction barriers have been measured for a number of transition metals.[5−13]

Theoretical studies have considerably contributed to the spectroscopic identification of the matrix-isolated products[16−22] and to the understanding of the nature of the chemical bonds in these species,[25−35] but only a few works have been devoted to explore the main features of the potential energy surfaces of M + CO_2 systems.[29,31,34,35] In the present paper, we focus on the gas phase oxygen abstraction reaction of the ground state Sc(^{2}D) with CO_2 and we attempt to describe the lowest energy reaction path from the Sc + CO_2 entrance channel toward the ScO + CO products.

Although the Sc + CO_2 → ScO + CO reaction is exothermic ($\Delta H° = -35.6$ kcal/mol),[36,37] it exhibits a nonnegligible activation barrier (2.9 kcal/mol)[9] as shown by kinetic experiments. Laser-ablated Sc atoms have been shown to give primarily the OScCO insertion product, but a very small amount of η^2_{CO} type Sc(CO_2) addition complexes has also been identified in the matrix isolation experiments.[17] These two species, however, seem to be associated with different potential energy surfaces, since density functional calculations[17,27,29,33] predicted the η^2_{CO} adduct to have $^2A'$ state, while the ground state of the OScCO product was found to be $^2A''$.[17,33] The $^2A'$ state of OScCO has also been considered in one of the theoretical studies,[29] and the equilibrium parameters reported for this state were fairly different from those obtained for $^2A''$. Because the η^2_{CO}-Sc(CO_2) and OScCO species are possible intermediates in the Sc + CO_2 → ScO + CO reaction, the above results suggest that at least two doublet state potential energy surfaces have to be considered to describe the full reaction path. The main goal of our present work was to map the details of the $^2A'$ and $^2A''$ potential energy surfaces.

II. Computational Details

The stationary points on the $^2A'$ and $^2A''$ surfaces were located using B3LYP density functional calculations.[38−40] The basis sets that we have chosen for these calculations include the (14,9,5)/[8,5,3] all electron Sc basis set from Schäfer, Horn, and Ahlrichs (SHA)[41] supplemented with two polarization p functions[42] and a diffuse d function[43] and the 6-311+G(2d) basis set[44] for carbon and oxygen. This basis set will be referred to as SHA+6-311+G(2d) in this paper.

The total energies of the located stationary points have been recalculated using a larger basis set, which is derived from the standard 6-311+(3df) set[45] by omitting the g polarization functions from the Sc basis. This basis set will hereafter be denoted as 6-311+(3df)′. Calculations with the standard 6-311+-(3df) basis set led to unphysical symmetry breaking of the molecular orbitals, which was not observed when the g functions were omitted from the original basis set. For each stationary point, we also carried out single-point CCSD(T) energy calcula-

* To whom correspondence should be addressed. I.P.: papai@chemres.hu. Y.H.: hannachi@cribx1.u-bordeaux.fr.

10.1021/jp025918m CCC: $22.00 © 2002 American Chemical Society
Published on Web 09/21/2002

TABLE 1: Optimized Geometries and Relative Energies Calculated at B3LYP/SHA+6-311+G(2d) Level[a]

	R_{ScO}	R_{ScC}	R_{CO}	$R_{CO'}$	$\alpha_{OCO'}$	α_{OScC}	$\alpha_{ScCO'}$	ϕ^b	ΔE^c	ZPE[d]	$\Delta E_{corr}{}^e$
					$^2A'$ surface						
$Sc(s^2d^1) + CO_2$			1.160	1.160	180.0				0.0	(7.3)	0.0
$TS_{ent}(^2A')$	2.344	3.119	1.180	1.150	175.4	18.9	144.5		1.9	(6.8)	1.4
η^2_{CO}-$Sc(CO_2)(^2A')$	1.898	2.115	1.386	1.189	127.4	40.0	171.1		−25.6	(6.4)	−26.5
$TS_{ins}(^2A')$	1.815	2.137	1.603	1.166	120.7	47.0	176.6		−24.3	(5.7)	−25.9
$TS_{oop}(^2A')$	1.698	2.467	2.585	1.124	122.3	74.2	161.4		−32.4	(5.4)	−34.3
$TS_{bend}(^2A')$	1.684	2.525	3.065	1.124	148.5	91.2	178.2		−31.8	(5.7)	−33.5
$OScCO(^2A')$	1.678	2.536	3.377	1.130	167.1	104.7	164.2		−32.0	(5.9)	−33.5
$ScO(^2\Sigma^+) + CO$	1.669			1.126					−27.7	(4.6)	−30.4
					$^2A''$ surface						
$Sc(s^2d^1) + CO_2$			1.160	1.160	180.0				0.0	(7.3)	0.0
$TS_{ent}(^2A'')$	2.298	3.078	1.183	1.150	173.5	19.3	146.6		2.1	(6.7)	1.5
η^2_{CO}-$Sc(CO_2)(^2A'')$	1.918	2.161	1.371	1.192	127.8	38.7	171.2		−16.9	(6.3)	−17.9
$TS_{ins}(^2A'')$	1.826	2.112	1.630	1.172	120.0	48.2	176.6		−14.9	(5.6)	−16.7
$OScCO(^2A'')$	1.690	2.217	3.268	1.157	151.5	112.8	179.9		−36.2	(5.6)	−37.9
TS_{iso}	1.673	2.516		1.161		110.4	93.4	93.9	−25.5	(4.5)	−28.3
OSc(CO)	1.685	2.366		1.198		119.4	68.2	95.6	−31.1	(5.2)	−33.2
$ScO(^2\Delta) + CO$[f]	1.669			1.126					5.7		3.0
					additional stationary points						
$\eta^2_{O,O}$-$Sc(CO_2)(^2A_1)$	1.935	2.342	1.347	1.347	111.4	35.1	55.7		−24.4	(5.7)	−26.0
$TS_{CO-OO}(^2A')$	2.002	3.048	1.293	1.194	131.7				−1.1	(6.0)	−2.4
$TS_{OO-diss}(^2A')$	1.778	2.435	1.742	1.222	106.5	45.6	59.6		−19.7	(5.3)	−21.7

[a] Units: bond lengths in Å, angles in degrees, energies in kcal/mol. [b] OScCO dihedral angle. [c] Relative energies with respect to $Sc(s^2d^1) + CO_2$. [d] Zero point vibrational energies. [e] ZPE-corrected relative energies. [f] The bond distance of $ScO(^2\Delta)$ has not been optimized.

tions[46,47] using the larger 6-311+(3df)′ basis set. The correlation treatment in the coupled cluster calculations involved all valence electrons, as well as the 3s and 3p electrons of Sc. The stability of the wave function was always checked to ensure that we indeed found the lowest energy solution in the self-consistent field procedure.

The vibrational frequencies were calculated at the B3LYP/SHA+6-311+G(2d) level for each stationary point, and they served as data to estimate the zero point energies (ZPE) and also to characterize the nature of the stationary points. To verify whether the located transition states connect the expected minima, intrinsic reaction coordinate (IRC) calculations[48] were carried out in both directions from each transition state.

The atomic populations (atomic charges, electron configurations, etc.) were derived by applying natural bond orbital (NBO) analysis[49] for the relevant structures. The relative stabilities of the intermediates are usually given relative to the $Sc(s^2d^1)+CO_2$ level. The ground state of the Sc atom was represented by a single determinant corresponding to the $(4s)^2\,(3d_{+1})^1$ occupation of spin orbitals. All calculations in the present study were performed using the Gaussian98 program.[50]

III. Results and Discussion

In the first part of this paper, we will thoroughly characterize the elementary steps of the title reaction. We start from the Sc + CO_2 entrance channel and follow the reaction path toward the final ScO + CO products. Previous theoretical studies on this system[27−29,33] indicated that the quartet states of various intermediates ($Sc(CO_2)$ and OScCO) lie well above the doublet states; it is therefore quite unlikely that intersystem crossings between doublet and quartet states occur in this reaction. We have thus considered only the lowest lying doublet state potential energy surfaces. In Table 1, we collected the relative energies and structural parameters calculated at the B3LYP/SHA+6-311G+(2d) level for each stationary point that we located. The optimized structures corresponding to these stationary points are illustrated in Figure 1. The B3LYP/SHA+6-311G+(2d) energy diagram for the entire Sc + CO_2 → ScO + CO reaction is depicted in Figure 2.

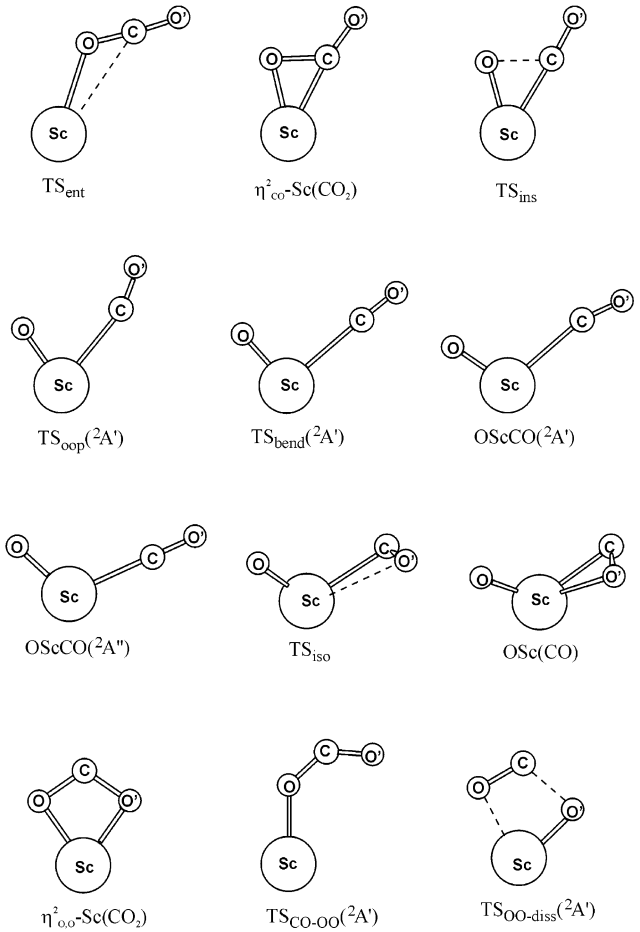

Figure 1. Structure and notation of the located stationary points.

A. En Route from Sc + CO_2 to ScO + CO. *A.1. Entrance Channel.* An interesting issue in the mechanism of any metal + ligand reaction is to understand how these reactions are initiated. Several recent theoretical studies[51−54] have raised this question for the interaction of transition metal atoms with small ligands such as N_2O and NO_2, but none of the studies reported

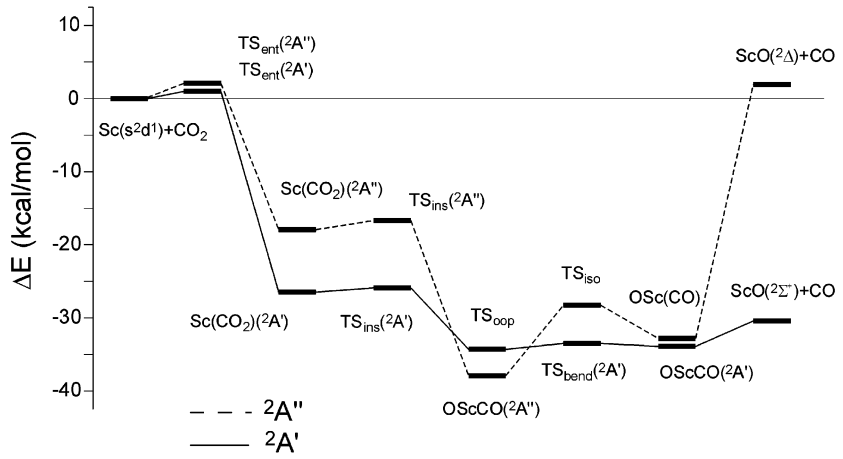

Figure 2. Energy diagram of the Sc + CO_2 → ScO + CO reaction based on ZPE-corrected B3LYP/SHA+6-311+G(2d) relative energies.

on M + CO_2 attempted to determine the approach barriers for CO_2 coordination.

We have located two transition states in the Sc + CO_2 entrance channel, corresponding to the $^2A'$ and $^2A''$ electronic states, whose unpaired electrons are associated with pure Sc 3d orbitals with a′ and a″ symmetry, respectively (see TS_{ent}-($^2A'$) and TS_{ent}($^2A''$) in Figures 1 and 2). Both electronic transition states lie about 1.5 kcal/mol above the reactants; therefore, they represent an entrance barrier for the reaction. The structure of these stationary points is very similar to that found for the analogue Sc + N_2O entrance transition state structure[54] in that in both cases the CO_2 and N_2O ligands are attacked on the O side by the metal atom (with R_{ScO} = 2.3 Å and $\alpha_{ScOC} = \alpha_{ScON}$ = 120°) and both ligands are only slightly bent. The NBO analysis shows no charge transfer between the reactants in these transition states; however, the electron configuration of the Sc atom is about $4s^{1.8}3d^{1.2}$ in both states, indicating a certain degree of s−d hybridization in the entrance transition structures. IRC calculations clearly revealed that the TS_{ent}($^2A'$) and TS_{ent}($^2A''$) transition states connect the Sc + CO_2 asymptote with the $^2A'$ and $^2A''$ states of the η^2_{CO}-Sc(CO_2) coordination complex. In an effort to find other routes to Sc−CO_2 coordination, first, we scanned the R_{ScC} and R_{ScO} distances for various arrangements of the Sc + CO_2 fragments but we could neither locate further transition states in the entrance channel nor find a barrierless path to the CO_2 coordination. We have also tried to locate a TS between Sc + CO_2 and the $\eta^2_{O,O}$-Sc(CO_2) complex, which was previously shown to be isoenergetic with the η^2_{CO} form,[27,33] but all of our attempts were unsuccessful. Of course, we cannot rule out the possibility of a direct pathway to $\eta^2_{O,O}$ coordination; however, it is quite likely that the TS_{ent}($^2A'$) and TS_{ent}($^2A''$) transition states represent the lowest energy barrier to CO_2 coordination. We note that the entropic effects would not change the relative rates of the two possible coordination routes because the activation entropies associated with the two entrance channels are estimated to be identical within 0.1 cal mol^{-1} K^{-1}.

A.2. CO_2 Coordination. The $^2A'$ and $^2A''$ surfaces tend to split after passing the entrance transition states, and the CO_2 coordination is accompanied with substantial energy stabilization. The stability of the two states of the η^2_{CO}-Sc(CO_2) complex is 26.5 ($^2A'$) and 17.9 kcal/mol ($^2A''$) relative to the reactants. To monitor the electronic rearrangements in the coordination process, we plotted the Sc atomic populations along the $^2A'$ IRC path (Figure 3).

Note first that the net atomic charge on the Sc atom (Q(Sc)) continuously increases from 0.0 to 1.0 when going from TS_{ent}-

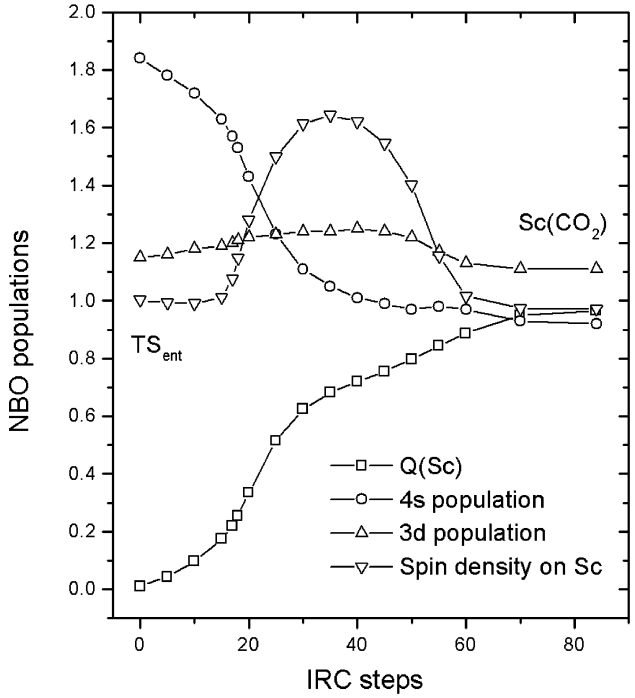

Figure 3. Sc atomic populations along the TS_{ent}($^2A'$) → η^2_{CO}-Sc(CO_2)-($^2A'$) IRC route.

($^2A'$) to η^2_{CO}-Sc(CO_2)($^2A'$), leading to an ionic $Sc^+(CO_2)^-$ species at the η^2_{CO} minimum. The total 3d population varies only in a narrow range along the IRC path; however, there is a sharp decrease in the 4s population already at the initial phase of the coordination route. The spin density of the Sc atom varies drastically in this region, and this is because the Sc → CO_2 electron transfer takes place in the manifold of minority (β or spin down) spin orbitals. In other words, the remaining 4s and 3d electrons are triplet coupled. The Sc 4s orbital becomes essentially singly occupied already at around step 30, where the Sc atom is still linked only to the oxygen end of CO_2 and the system is stabilized only by 8 kcal/mol with respect to TS_{ent}-($^2A'$). This underlines the importance of the metal → ligand electron transfer in the initial phase of the CO_2 coordination, which is in line with the mechanism suggested recently by Stirling for the interaction of transition metal atoms with nitrogen oxides.[53] We feel that it is important to point out here that the coordination process is adiabatic in a sense that no surface crossing is encountered going from TS_{ent}($^2A'$) to η^2_{CO}-Sc(CO_2)($^2A'$) (or from TS_{ent}($^2A''$) to η^2_{CO}-Sc(CO_2)($^2A''$)), the

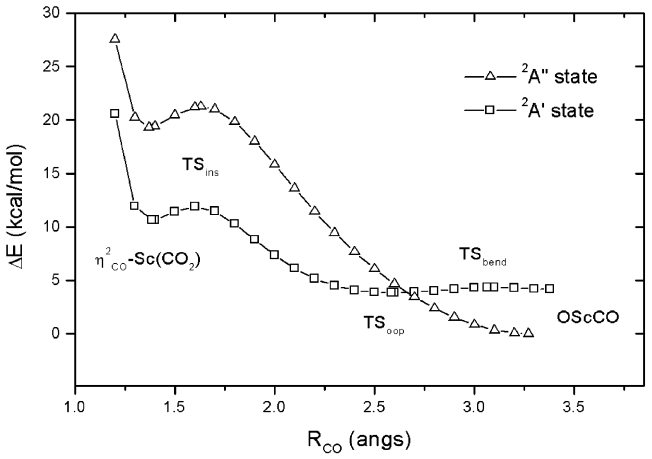

Figure 4. ^{2}A′ and ^{2}A″ potential energy curves for the η^2_{CO}-Sc(CO_2) → OScCO insertion. Energies are with respect to the OScCO(^{2}A″) species.

system remains on the same potential surface. The second half of the path is characterized by the diminution of the spin density of Sc, which is attributed to the development of the covalent contribution of the metal−ligand bonding, which is also characteristic of the metal−CO_2 interaction in the η^2_{CO} form of M(CO_2) complexes as described previously.[27,31,33] The unpaired electron of the ^{2}A′ state of η^2_{CO}-Sc(CO_2) is localized on Sc and is associated with an s−d hybrid (a′) orbital.

The CO_2 coordination on the ^{2}A″ surface is also governed by the Sc → CO_2 electron transfer; however, the out-of-plane a″(3d) orbital is not involved in the s−d hybridization. The hybridization can only be attained through 4s → 3d promotion resulting in a less stable ^{2}A″ state η^2_{CO} complex as compared to ^{2}A′. The 4s → 3d promotion in the ^{2}A″ state of η^2_{CO}-Sc(CO_2) is apparent from the NBO populations: the electronic configuration of Sc in ^{2}A″ is $4s^{0.5}3d^{1.5}$ while it is $4s^{0.9}3d^{1.1}$ in the ^{2}A′ state of η^2_{CO}-Sc(CO_2).

Our B3LYP/SHA+6-311+G(2d) calculations predict the $\eta^2_{O,O}$-Sc(CO_2) complex to be bound by 26 kcal/mol relative to Sc + CO_2. We located a transition state TS_{CO-OO}(^{2}A′) on the ^{2}A′ surface that connects the η^2_{CO} and $\eta^2_{O,O}$ forms, but the η^2_{CO} → $\eta^2_{O,O}$ isomerization should be kinetically hindered because the TS_{CO-OO}(^{2}A′) transition state lies about 24 kcal/mol above the η^2_{CO}-Sc(CO_2)(^{2}A′) and $\eta^2_{O,O}$-Sc(CO_2)(^{2}A′) minima.

A.3. Scandium Insertion. Similarly to what we found for the Ti + CO_2 and V + CO_2 systems,[31,35] the η^2_{CO}-Sc(CO_2) complex is a metastable state on the ^{2}A′ and ^{2}A″ surfaces, because the insertion of the Sc atom into the coordinated CO bond can easily occur. The insertion paths are illustrated in Figure 4, where we depicted the ^{2}A′ and ^{2}A″ potential energy curves as a function of the cleaved C−O bond distance (R_{CO}) derived from constrained geometry optimizations. The barriers to Sc insertion, related to the "reactant-like" TS_{ins}(^{2}A′) and TS_{ins}(^{2}A″) transition states, are negligible; they are calculated to be only 0.6 and 1.2 kcal/mol on the ^{2}A′ and ^{2}A″ surfaces, respectively. It is clearly seen in Figure 4 that the energy stabilization on the ^{2}A″ insertion path is significantly larger than on the ^{2}A′ surface, resulting in a ^{2}A′−^{2}A″ surface crossing at around R_{CO} = 2.7 Å. The flat nature of the ^{2}A′ potential energy curve in the 2.4 Å < R_{CO} < 3.4 Å region represents another striking difference between the two insertion paths.

As pointed out previously,[29,31] the thermodynamic driving force of the M + CO_2 → OMCO insertion reactions for early transition metals is the formation of a strong metal−oxygen bond in the insertion process and the OMCO products are viewed as carbonyl complexes of diatomic MO species. The enhanced exothermicity of the ^{2}A″ insertion path and the flat nature of the ^{2}A′ curve are closely related to the strength of the OM−CO bond. The insertion reaction along the ^{2}A′ surface yields ground state ($^2\Sigma^+$) ScO species, whose unpaired electron occupies an essentially pure Sc 4s orbital. For symmetry reasons, this orbital does not participate in a π type stabilizing metal → CO charge transfer; therefore, ScO($^2\Sigma^+$) forms only a very weak association complex with the CO molecule. On the other hand, the ^{2}A″ insertion path correlates with an excited state ($^2\Delta$) of ScO having a singly occupied δ type orbital localized on the Sc atom; thus, the metal−CO (δ(Sc)-π*(CO)) back-bonding is symmetry allowed in a bent arrangement and the ^{2}A″ system is stabilized by this interaction. The NBO analysis confirms this trend: the total charge on the CO molecule in the OScCO-(^{2}A″) insertion product is calculated to be $Q_{CO} = -0.43$, whereas the carbonyl group in OScCO(^{2}A′) is close to neutral ($Q_{CO} = -0.08$).

A.4. Insertion Products. The ^{2}A′ insertion route has already been investigated previously by Sodupe et al.[29] The OScCO-(^{2}A′) product in that work was characterized by an imaginary vibrational frequency corresponding to the out-of-plane distortion of the C_s structure. This stationary point is labeled TS_{oop}-(^{2}A′) in Figure 4, and it represents a very shallow minimum on the ^{2}A′ potential energy curve. We located two other stationary points on the ^{2}A′ curve by increasing the R_{CO} distance, namely, the TS_{bend}(^{2}A′) transition state and the OScCO(^{2}A′) minimum (see also Figure 1 and Table 1). TS_{bend}(^{2}A′) is a transition structure with respect to the in-plane OScC bending motion, while OScCO(^{2}A′) is a real minimum on the potential energy surface being 4.4 kcal/mol less stable than the OScCO(^{2}A″) product. This latter complex is reached directly from TS_{ins}(^{2}A″) on the ^{2}A″ surface. Our calculations indicate that the OScCO-(^{2}A′) structure does not correspond to the global minimum of the ^{2}A′ surface since the TS_{oop}(^{2}A′) structure is slightly below in energy (see Table 1). We carried out geometry optimization from a slightly distorted TS_{oop}(^{2}A′) structure without the C_s symmetry constraint, but these calculations variationally collapsed to the ^{2}A″ state and converged to the OScCO(^{2}A″) product. As seen in Figure 4, the TS_{oop}(^{2}A′) stationary point is in the close vicinity of the ^{2}A′−^{2}A″ surface crossing, which might be a likely reason for having difficulties in locating a possible C_1 minimum in this region.

Our B3LYP/SHA+6-311+G(2d) calculations have also revealed that the OScCO(^{2}A″) insertion product can isomerize to an asymmetrical structure (labeled OSc(CO) in Figures 1 and 2) corresponding to the side-bonded CO molecule. This isomer is identical to that called OSc(η^2-CO) in ref 17, but it clearly does not have a ^{2}A′ ground state as given in that paper because (i) this structure has no symmetry and (ii) it is directly connected to the OScCO(^{2}A″) minimum via the TS_{iso} transition state rather than to the ^{2}A′ surface (see Figures 1 and 2 and Table 1). The barrier to OScCO(^{2}A″) → OSc(CO) isomerization is predicted to be 9.6 kcal/mol at the present level of theory, and it is 4.9 kcal/mol in the reverse direction. The OSc(CO) isomer is also stabilized by the δ(Sc)-π*(CO) back-bonding only in a different arrangement of the ScO and CO subunits as indicated in Figure 5. The side-bonded CO complexes are quite rare in the family of metal−carbonyl species, but the existence of OSc(CO) has clearly been demonstrated in the work cited above.

A.5. CO Detachment. The exit channel of the Sc + CO_2 → ScO + CO oxygen abstraction reaction corresponds to the dissociation of the CO molecule from the insertion product. The energy diagram shown in Figure 2 indicates that the dissociation

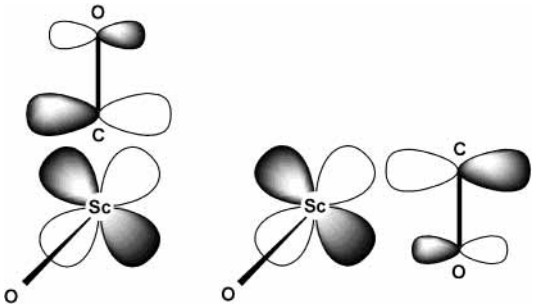

Figure 5. δ(Sc)-π^*(CO) interactions in OScCO(^{2}A″) and OSc(CO).

is feasible only on the ^{2}A′ surface. As expected, the weakly bound OScCO(^{2}A′) complex can easily dissociate into ScO($^2\Sigma^+$) + CO; however, because of a large $^2\Sigma^+ - {}^2\Delta$ energy separation in ScO (the measured splitting is 40.6 kcal/mol),[55] the decomposition of the OScCO(^{2}A″) and OSc(CO) intermediates is energetically prohibited.

The dissociation energy of the OScCO(^{2}A′) complex is predicted to be only 3.1 kcal/mol in the B3LYP/SHA+6-311+G(2d) calculations, whereas the OScCO(^{2}A″) and OSc(CO) insertion products are calculated to be bound by 41.9 and 36.8 kcal/mol with respect to the ScO($^2\Delta$) + CO dissociation asymptote. We found no exit barrier on the ^{2}A′ surface, and our calculations show that the lowest energy dissociation route from the OScCO(^{2}A″) complex corresponds to OScCO(^{2}A″) → OSc(CO) isomerization followed by barrierless dissociation.

It is interesting to note that the $\eta^2_{O,O}$-Sc(CO_2)($^2A_1$) coordination complex can also easily dissociate into ScO($^2\Sigma^+$) + CO, passing a transition state ($TS_{O,O-diss}$(^{2}A′) in Table 1), which lies only 4.3 kcal/mol above $\eta^2_{O,O}$-Sc(CO_2)($^2A_1$). This activation energy is much smaller than that found for the dissociation of the $\eta^2_{O,O}$-Ni(CO_2) ($^3B_1$) cyclic complex by Mebel et al.[34] The barrier for the reverse route (ScO($^2\Sigma^+$) + CO → $\eta^2_{O,O}$-Sc(CO_2)-($^2A_1$)) is predicted to be 8.7 kcal/mol, pointing to a possible way of $\eta^2_{O,O}$-Sc(CO_2) formation at higher temperature.

B. Overall Energetics at Higher Levels. To summarize the results of the previous section, we note that the ^{2}A′ and ^{2}A″ potential energy surfaces represent two distinct reaction paths for the Sc + CO_2 system. Both pathways lead to the insertion of Sc into a C−O bond, which is initiated by the η^2_{CO} coordination of the CO_2 molecule. Of the two possible insertion products, the OScCO(^{2}A′) complex is only weakly bound; however, the OScCO(^{2}A″) species is rather stable with respect to its dissociation limit. Although both surfaces correlate with the Sc(s^2d^1) + CO_2 ground state reactants, the degree of 4s−3d hybridization and the 4s → 3d promotion characteristic of the Sc atom is quite different along the two routes. Because current approximate DFT methods fail to provide accurate atomic excitation energies,[56−59] one may wonder if the overall energetics obtained at the B3LYP/SHA+6-311+G(2d) level represent reliable predictions. To this end, we recalculated the total energies of all stationary points at the B3LYP/6-311+G-(3df)′ and CCSD(T)/6-311+G(3df)′ levels using the B3LYP/SHA+6-311+G(2d)-optimized geometries (for basis set notation, see Computational Details). The calculated energies are summarized in Table 2, and the energy diagram corresponding to the CCSD(T)/6-311+G(3df)′ results is shown in Figure 6.

In agreement with a general belief that density functional calculations are less sensitive to the quality of the basis set than the correlated ab initio methods,[60] we found only a slight variation in the relative energies when going from B3LYP/SHA+6-311+G(2d) to B3LYP/6-311+G(3df)′ calculations. The deviation between the two sets of results is at most 1.4 kcal/mol (the mean deviation is only 0.6 kcal/mol), indicating that the B3LYP/SHA+6-311+G(2d) relative energies can essentially be considered as converged B3LYP results with respect to the basis set.

TABLE 2: ZPE Corrected Relative Energies (in kcal/mol) of Stationary Points Calculated at Various Levels of Theory[a]

	B3LYP/SHA+ 6-311+G(2d)	B3LYP/6-311+ G(3df)′	CCSD(T)/6-311+ G(3df)′
	^{2}A′ surface		
Sc(s^2d^1) + CO_2	0.0	0.0	0.0
TS_{ent}(^{2}A′)	1.4	0.7	1.8
Sc(CO_2)-η^2_{CO}(^{2}A′)	−26.5	−25.4	−19.0
TS_{ins}(^{2}A′)	−25.9	−25.6	−20.4
TS_{oop}(^{2}A′)	−34.3	−34.6	−34.6
TS_{bend}(^{2}A′)	−33.5	−33.1	−33.9
OScCO(^{2}A′)	−33.5	−33.9	−32.5
ScO($^2\Sigma$) + CO	−30.4	−30.6	−30.6
	^{2}A″ surface		
Sc(s^2d^1) + CO_2	0.0	0.0	0.0
TS_{ent}(^{2}A″)	1.5	1.9	2.3
Sc(CO_2)-η^2_{CO}(^{2}A″)	−17.9	−18.0	−7.7
TS_{ins}(^{2}A″)	−16.7	−16.4	−6.7
OScCO(^{2}A″)	−37.9	−36.5	−29.1
TS_{iso}	−28.3	−26.6	−22.0
OSc(CO)	−33.2	−33.6	−26.5
ScO($^2\Delta$) + CO[b]	3.0	1.7	13.5

[a] ZPE corrections from B3LYP/SHA+6-311+G(2d) vibrational data. [b] Estimated from the vertical $^2\Sigma^+ - {}^2\Delta$ excitation energies.

The comparison of the B3LYP/6-311+G(3df)′ and CCSD-(T)/6-311+G(3df)′ energies, however, shows notable differences. Although the two methods provide identical Sc(s^2d^1) + CO_2 → ScO($^2\Sigma^+$) + CO reaction energies (30.6 kcal/mol), we see significant variations in the relative energies of the intermediates. Note for example that the CCSD(T) calculations predict consistently larger energy separations between the ^{2}A′ and the ^{2}A″ states for the intermediates, and as a result, the ^{2}A′ and ^{2}A″ surfaces do not intersect in the region of insertion products. Because the ^{2}A″ state potential energy surface is characterized by a larger 3d population of the Sc atom as compared to ^{2}A′, the discrepancy between the B3LYP and the CCSD(T) results can be attributed to the well-known tendency of currently available approximate exchange−correlation functionals (including the B3LYP functional) to unduly overestimate the stability of d-rich configurations in transition metal atoms and ions.[56−59] For instance, the $4s^23d^1$ → $4s^13d^2$ excitation in a Sc atom is predicted to be 18.0 and 34.1 kcal/mol at the B3LYP/6-311+G(3df)′ and CCSD(T)/6-311+G(3df)′ levels, whereas the experimental value is 33.0 kcal/mol.[61] The results obtained for the $^2\Sigma^+ - {}^2\Delta$ splitting in the ScO product also indicate that the relative position of the ^{2}A′ and ^{2}A″ surfaces might be less accurately represented in B3LYP calculations. For the vertical $^2\Sigma^+ - {}^2\Delta$ excitation energy, B3LYP/6-311+G(3df)′ calculations give 32.3 kcal/mol, whereas the measured value is 40.6 kcal/mol.[55] The CCSD(T)/6-311+G(3df)′ prediction for the vertical excitation is 44.1 kcal/mol.

In a previous theoretical work,[28] the performance of various density functional and coupled cluster methods for the stability of the $\eta^2_{O,O}$-Sc(CO_2) complex has been thoroughly examined. The authors found that DFT methods predict more stable Sc-(CO_2) complexes as compared to CCSD(T), because they overestimate the electron affinity of the CO_2 molecule and, as already mentioned above, they provide too small 4s → 3d promotion energies. Given that the present B3LYP/6-311+G-(3df)′ and CCSD(T)/6-311+G(3df)′ predictions for the adiabatic electron affinity of CO_2 are −0.34 and −0.66 eV, respectively (the experimental value is −0.6 eV),[62] it is not surprising to see that the two methods give quite different stabilities for the

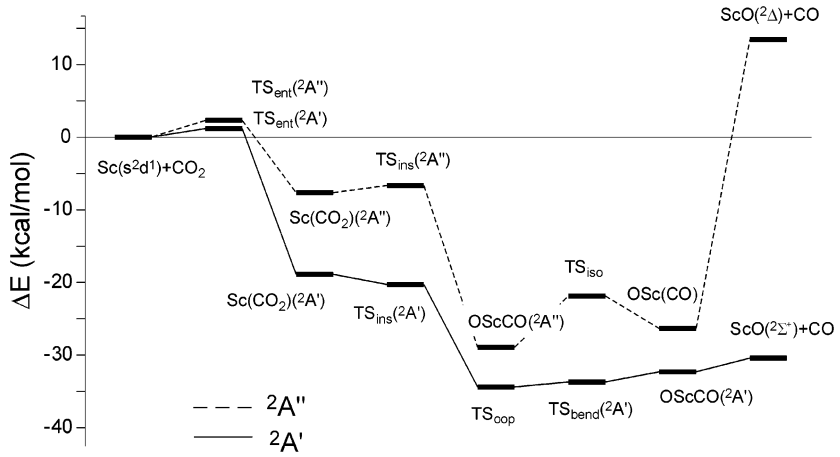

Figure 6. Energy diagram of the Sc + CO_2 → ScO + CO reaction based on ZPE-corrected CCSD(T)/6-311+G(3df)′ relative energies.

$^2A'$ and $^2A''$ states of the η^2_{CO}-Sc(CO_2) complex. Because there are only slight variations in the electron configuration of the Sc atom along the η^2_{CO}-Sc(CO_2) → OScCO insertion part of the reaction, the energetics of the insertion process (for a given potential surface) appears to be consistent at the B3LYP and CCSD(T) levels. Nevertheless, we can conclude that the coupled cluster energy predictions represent more reliable results for the overall energetics of the Sc + CO_2 → ScO + CO reaction.

C. Relevance to Experimental Data. Finally, we wish to relate the presented theoretical results to available experimental findings. Let us recall first that the ZPE-corrected Sc(s^2d^1) + CO_2 → ScO($^2\Sigma^+$) + CO reaction energies predicted by the B3LYP/6-311+G(3df)′ and CCSD(T)/6-311+G(3df)′ methods are equally 30.6 kcal/mol, which slightly underestimate the experimental reaction heat (35.6 kcal/mol)[9] derived from the thermochemical data given in the JANAF Tables.[37]

Our results indicate that the rate-determining step in the Sc(s^2d^1) + CO_2 → ScO($^2\Sigma^+$) + CO reaction corresponds to the CO_2 coordination; therefore, the height of the entrance channel barrier can be directly related to the activation energy deduced in the temperature-dependent gas phase kinetic study by Campbell and co-workers.[9] Our best estimates (ZPE-corrected CCSD(T)/6-311+G(3df)′ results) for the approach barrier are 1.8 ($TS_{ent}(^2A')$) and 2.3 ($TS_{ent}(^2A'')$) kcal/mol, which are reasonably close to the experimental estimate (2.9 kcal/mol).[9]

The overall energetics of the reaction provides new insight into the interpretation of the results of matrix isolation experiments.[17] Because the $^2A'$ and $^2A''$ reaction channels are almost equally accessible in the Sc + CO_2 system, the full oxygen abstraction reaction and the formation of the ground state OScCO insertion product can simultaneously be accomplished. Indeed, the main product identified in the reactions of laser-ablated Sc atom with CO_2 was OScCO($^2A''$), but the formation of the ScO($^2\Sigma^+$) and CO products was also observed. The reversible photoisomerization of OScCO($^2A''$) to the side-bonded OSc(CO) species can also be rationalized, since the two isomers lie on the same energy surface and they are separated by a relatively small energy barrier. The fact that the $\eta^2_{O,O}$-Sc(CO_2) complex was not observed in the matrix isolation experiments is consistent with our findings in that we showed this species to undergo a fast ScO($^2\Sigma^+$) + CO dissociation. Interestingly, a minor amount of the η^2_{CO}-Sc(CO_2) coordination complex was found to be present among the isolated products, although present calculations predict this species to lie in at most an extremely shallow minimum on both $^2A'$ and $^2A''$ surfaces.

IV. Concluding Remarks

We showed in this paper that both $^2A'$ and $^2A''$ state Sc + CO_2 reactions lead to spontaneous metal insertion into CO_2; however, only the $^2A'$ state insertion complex can readily dissociate into ScO + CO. The entrance channel of the Sc + CO_2 → ScO + CO reaction corresponds to the η^2_{CO} coordination of the CO_2 molecule, which is initiated by the Sc → CO_2 electron transfer in an early stage of the coordination process. The approach barrier estimated from our calculations agrees reasonably well with the measured activation energy of the Sc + CO_2 → ScO + CO gas phase reaction. The two matrix-isolated isomers of the OSc−CO insertion products were shown to correlate with the ScO($^2\Delta$) + CO dissociation limit lying far above the ground state ScO($^2\Sigma^+$) + CO asymptote.

Shortly before finishing this paper, a new theoretical work on the Ti + CO_2 reaction appeared in the literature.[63] In their paper, Hwang and Mebel give a detailed account of possible intermediates, but they found no barrier to η^2_{CO} coordination. The authors also mentioned that their recent DFT calculations on Sc + CO_2[64] indicate no entrance channel barrier for the η^2_{CO} coordination and the existence of a 3.2 kcal/mol barrier toward the $\eta^2_{O,O}$ coordination. Our present work may give new insight to the mechanism of the insertion route.

Acknowledgment. This work has been supported in part by a Hungarian−French joint research program (TéT, F-5/99; Balaton 2000/00851QL) and by the Hungarian Research Foundation (OTKA, F037345). J.M. acknowledges the allocation of computer time by CNRS through IDRIS (Project 11441). We thank A. Mebel for providing a copy of their Sc + CO_2 manuscript prior to publication.

References and Notes

(1) Braunstein, P.; Matt, D.; Nobel, D. *Chem. Rev.* **1988**, *88*, 747.
(2) Aresta, M.; Quaranta, E.; Tommasi, I. *New. J. Chem.* **1994**, *18*, 133.
(3) Gibson, D. H. *Chem. Rev.* **1996**, *96*, 2063.
(4) Yin, X.; Moss, J. R. *Coord. Chem. Rev.* **1999**, *181*, 27.
(5) McClean, R. E.; Pasternack, L. *J. Phys. Chem.* **1992**, *96*, 9828.
(6) Campbell, M. L.; McClean, R. E. *J. Phys. Chem.* **1993**, *97*, 7942.
(7) McClean, R. E.; Campbell, M. L.; Goodwin, R. H. *J. Phys. Chem.* **1996**, *100*, 7502.
(8) McClean, R. E.; Campbell, M. L.; Kolsch, E. J. *J. Phys. Chem. A* **1997**, *101*, 3348.
(9) Campbell, M. L.; Hooper, K. L.; Kolsch, E. J. *Chem. Phys. Lett.* **1997**, *274*, 7.
(10) Campbell, M. L.; Hooper, K. L. *J. Chem. Soc., Faraday Trans.* **1997**, *93*, 2139.
(11) Campbell, M. L. *Chem. Phys. Lett.* **1998**, *294*, 339.
(12) Campbell, M. L. *J. Chem. Soc., Faraday Trans.* **1998**, *934*, 1687.

(13) Campbell, M. L. *Phys. Chem. Chem. Phys.* **1999**, *1*, 3731.
(14) Mascetti, J.; Tranquille, M. *J. Phys. Chem.* **1988**, *92*, 2177.
(15) Chertihin, G. V.; Andrews, L. *J. Am. Chem. Soc.* **1995**, *117*, 1595.
(16) Souter, P. F.; Andrews, L. *J. Am. Chem. Soc.* **1997**, *119*, 7350.
(17) Zhou, M.; Andrews, L. *J. Am. Chem. Soc.* **1998**, *120*, 13230.
(18) Zhou, M.; Liang, B.; Andrews, L. *J. Phys. Chem. A* **1999**, *103*, 2013.
(19) Zhou, M.; Andrews, L. *J. Phys. Chem. A* **1999**, *103*, 2066.
(20) Wang, X.; Chen, M.; Zhang, L.; Qin, Q. *J. Phys. Chem. A* **2000**, *104*, 758.
(21) Chen, M.; Wang, X.; Zhang, L.; Qin, Q. *J. Phys. Chem. A* **2000**, *104*, 7010.
(22) Liang, B.; Andrews, L. *J. Phys. Chem. A* **2002**, *106*, 595.
(23) Caballol, R.; Marcos, E. S.; Barthelat, J. *J. Phys. Chem.* **1987**, *91*, 1328.
(24) Jeung, G. H. *Mol. Phys.* **1988**, *65*, 669.
(25) Jeung, G. H. *Mol. Phys.* **1989**, *67*, 747.
(26) Jeung, G. H. *Chem. Phys. Lett.* **1995**, *232*, 319.
(27) Sodupe, M.; Branchadell, V.; Oliva, A. *J. Phys. Chem.* **1995**, *99*, 8567.
(28) Rodriguez-Santiago, L.; Sodupe, M.; Branchadell, V. *J. Chem. Phys.* **1996**, *105*, 9966.
(29) Sodupe, M.; Branchadell, V.; Oliva, A. *J. Mol. Sruct.* **1996**, *371*, 79.
(30) Galan, F.; Fouassier, M.; Tranquille, M.; Mascetti, J.; Papai, I. *J. Phys. Chem. A* **1997**, *101*, 2626.
(31) Papai, I.; Mascetti, J.; Fournier R. *J. Phys. Chem. A* **1997**, *101*, 4465.
(32) Mascetti, J.; Galan, F.; Papai, I. *J. Coord. Chem. Rev.* **1999**, *190*−*192*, 557.
(33) Mele, F.; Russo, N.; Toscano, M.; Illas, F. In *New Trends in Quantum Systems in Chemistry and Physics*; Maruani, J., Ed.; Kluwer: Dordrecht, 2000; Vol. 2.
(34) Mebel, A. M.; Hwang, D. *J. Phys. Chem. A* **2000**, *104*, 11622.
(35) Papai, I.; Hannachi, Y.; Gwizdala, S.; Mascetti, J. *J. Phys. Chem. A* **2002**, *106*, 4181.
(36) Pedley, J. B.; Marshall, E. M. *J. Phys. Chem. Ref. Data* **1983**, *12*, 967.
(37) Chase, M. W., Jr.; Davies, C. A.; Downey, J. R., Jr.; Frurip, D. J.; McDonald, R. J.; Syverud, A. N. JANAF Thermochemical Tables, 3rd ed. *J. Phys. Chem. Ref. Data* **1985**, *14* (Suppl. 1).
(38) Becke, A. D. *J. Chem. Phys.* **1993**, *98*, 5648.
(39) Lee, C.; Yang, W.; Parr, R. G. *Phys. Rev. B* **1988**, *37*, 785.
(40) Stephens, P. J.; Devlin, F. J.; Chabalowski, C. F.; Frisch, M. J. *J. Phys. Chem.* **1994**, *98*, 11623.
(41) Schäfer, A.; Horn, H.; Ahlrichs, R. J. *Chem. Phys.* **1992**, *97*, 2571.
(42) Wachters, A. J. H. *J. Chem. Phys.* **1970**, *52*, 1033.
(43) Hay, P. J. *J. Phys. Chem.* **1977**, *66*, 43.
(44) Krishnan, R.; Binkley, J. S.; Seeger, R.; Pople, J. A. *J. Chem. Phys.* **1980**, *72*, 650. (b) Frisch, M. J.; Pople, J. A.; Binkley, J. S. *J. Chem. Phys.* **1984**, *80*, 3265.
(45) See ref 50.
(46) Purvis, G. D.; Bartlett, R. J. *J. Chem. Phys.* **1982**, *76*, 1910.
(47) Pople, J. A.; Head-Gordon, M.; Raghavachari, K. *J. Chem. Phys.* **1987**, *87*, 5968.
(48) Gonzalez, C.; Schlegel, H. B. *J. Chem. Phys.* **1989**, *90*, 2154.
(49) Reed, A. E.; Curtiss, L. A.; Weinhold, F. *Chem. Rev.* **1988**, *88*, 899.
(50) Frisch, M. J.; Trucks, G. W.; Schlegel, H. B.; Gill, P. M. W.; Johnson, B. G.; Robb, M. A.; Cheeseman, J. R.; Keith, T.; Petersson, G. A.; Montgomery, J. A.; Raghavachari, K.; Al-Laham, M. A.; Zakrzewski, V. G.; Ortiz, J. V.; Foresman, J. B.; Cioslowski, J.; Stefanov, B. B.; Nanayakkara, A.; Challacombe, M.; Peng, C. Y.; Ayala, P. Y.; Chen, W.; Wong, M. W.; Andres, J. L.; Replogle, E. S.; Gomperts, R.; Martin, R. L.; Fox, D. J.; Binkley, J. S.; Defrees, D. J.; Baker, J.; Stewart, J. P.; Head-Gordon, M.; Gonzalez, C.; Pople, J. A. *Gaussian 94*; Gaussian, Inc.: Pittsburgh, PA, 1995. (b) Frisch, M. J.; Trucks, G. W.; Schlegel, H. B.; Scuseria, G. E.; Robb, M. A.; Cheeseman, J. R.; Zakrzewski, V. G.; Montgomery, J. A., Jr.; Stratmann, R. E.; Burant, J. C.; Dapprich, S.; Millam, J. M.; Daniels, A. D.; Kudin, K. N.; Strain, M. C.; Farkas, O.; Tomasi, J.; Barone, V.; Cossi, M.; Cammi, R.; Mennucci, B.; Pomelli, C.; Adamo, C.; Clifford, S.; Ochterski, J.; Petersson, G. A.; Ayala, P. Y.; Cui, Q.; Morokuma, K.; Malick, D. K.; Rabuck, A. D.; Raghavachari, K.; Foresman, J. B.; Cioslowski, J.; Ortiz, J. V.; Stefanov, B. B.; Liu, G.; Liashenko, A.; Piskorz, P.; Komaromi, I.; Gomperts, R.; Martin, R. L.; Fox, D. J.; Keith, T.; Al-Laham, M. A.; Peng, C. Y.; Nanayakkara, A.; Gonzalez, C.; Challacombe, M.; Gill, P. M. W.; Johnson, B. G.; Chen, W.; Wong, M. W.; Andres, J. L.; Head-Gordon, M.; Replogle, E. S.; Pople, J. A. *Gaussian 98*, revision A.9; Gaussian, Inc.: Pittsburgh, PA, 1998.
(51) Stirling, A. *J. Phys. Chem. A* **1998**, *102*, 6565.
(52) Stirling, A. *Chem. Phys. Lett.* **1998**, *298*, 101.
(53) Stirling, A. *J. Am. Chem. Soc.* **2002**, *124*, 4058.
(54) Delabie, A.; Vinckier, C.; Flock, M.; Pierloot, K. *J. Phys. Chem. A* **2001**, *105*, 5479.
(55) Wu, H.; Wang, L. *J. Phys. Chem. A* **1998**, *102*, 9129.
(56) Kutzler, F. W.; Painter, G. S. *Phys. Rev. B* **1991**, *43*, 6865.
(57) Russo, T. V.; Martin, R. L.; Hay, P. J. *J. Chem. Phys.* **1994**, *101*, 7729.
(58) Holthausen, M. C.; Mohr, M.; Koch, W. *Chem. Phys. Lett.* **1995**, *240*, 245.
(59) Yanagisawa, S.; Tsuneda, T.; Hirao, K. *J. Chem. Phys.* **2000**, *112*, 545.
(60) Bauschlicher, C. W.; Ricca, A.; Partridge, H.; Lamghoff, S. R. In *Recent Advances in Density Functional Methods (Part II)*; Chong, D. P., Ed.; World Scientific: Singapore, 1997.
(61) Martin, R. L.; Hay, P. J. *J. Chem. Phys.* **1981**, *75*, 4539.
(62) Compton, R. N.; Reinhardt, P. W.; Cooper, C. D. *J. Chem. Phys.* **1975**, *63*, 3821.
(63) Mebel, A. M.; Hwang, D. Y. *J. Chem. Phys.* **2002**, *116*, 5633.
(64) Hwang, D. Y.; Mebel, A. M. *Chem. Phys. Lett.* **2002**, *357*, 51.